Chapter 2
Remote Sensing of Coastal Hazards

Victor V. Klemas

Abstract With the coastal population increasing, storms have been inflicting unprecedented losses on coastal communities. Coastal agencies require advance information on the predicted path, intensity and progress of a storm and associated waves and storm surges; near-real-time information during the peak of the storm to monitor flooding and control rescue operations; and post-storm reports to assess the damage and plan the recovery. The same holds true for other disasters, such as oil spills and algal blooms. Coastal communities are also facing a rising sea level, caused mainly by global warming. Airborne and satellite remote sensors, such as multispectral imagers, Lidar and radar, are now able to provide most of the information required for emergency response and coastal management.

2.1 Introduction

More than half of the U.S. population lives in the coastal zone. With events such as the hurricanes of 2004 and 2005, annual losses to coastal communities can total billions of dollars. Environmental impacts from coastal storms include beach erosion, wetland destruction, excessive nutrient loading, algal blooms, hypoxia and anoxia, fish kills, large scale releases of pollutants and debris, and spread of pathogens.

Over the long term, coastal communities are also facing a rising sea level. The sea level is rising because water expands as it is warmed and because water from melting glaciers and ice sheets is added to the oceans. The substantial sea level rise and more frequent storms predicted for the next 50–100 years will affect coastal towns and roads, coastal economic development, beach erosion control strategies,

V.V. Klemas (✉)
School of Marine Science and Policy, University of Delaware, Newark, DE 19716, USA
e-mail: klemas@udel.edu

C.W. Finkl (ed.), *Coastal Hazards*, Coastal Research Library 6,
DOI 10.1007/978-94-007-5234-4_2,

salinity of estuaries and aquifers, coastal drainage and sewage systems, and coastal wetlands and coral reefs (Gesch 2009; IPCC 2007; NOAA 1999).

Because the coastal population continues to increase and road improvements have not kept up with this rapid population growth, more time is needed to carry out an evacuation. As a result, coastal and emergency managers need advance information on the predicted path, intensity and progress of a storm and associated waves and storm surge, near-real-time information during the peak of the storm to monitor flooding and control rescue operations, and post-storm reports to assess the damage, plan urban recovery, restore power lines and roads, and to improve levees and drainage canals (NASA 2005; NASA/GSFC 2010).

Airborne and satellite remote sensors are providing the required information together with observers in aircraft and on the ground. During Hurricane Katrina in 2005, remote sensing played a major role in tracking the storm and the devastation it left behind in urban New Orleans and surrounding wetlands (Hayes 2005; Klemas 2009; Rykhus 2005; Stone and Muller 2005). For instance, airborne Lidar data sets were used to perform a regional storm tide inundation analysis of Hurricane Katrina (Stoker et al. 2009).

Detailed technical descriptions of satellite and airborne remote sensing systems and their capabilities are contained in various other publications (Jensen 2007; Martin 2004; Purkis and Klemas 2011; Robinson 2004). The objective of this article is to review practical applications of remote sensing for monitoring coastal hazards, including storms, algal blooms, oil spills, and mapping their environmental impacts.

2.2 Monitoring Storm Surge and Flooding

One important model used by the National Oceanic and Atmospheric Administration (NOAA) National Hurricane Center to estimate storm surge heights and winds resulting from hurricanes is the SLOSH (Sea, Lake, and Overland Surges from Hurricanes) model. It takes into account the pressure, size, forward speed, track, and winds of a hurricane. SLOSH is used to evaluate the threat from storm surges, and emergency managers use these data to determine which areas must be evacuated. SLOSH model results are combined with road network and traffic flow information, rainfall amounts, river flow, and wind-driven waves to identify at-risk areas (NOAA/CSC 2008).

If the SLOSH model is used to estimate storm surge for an actual, predicted hurricane, forecast data must be put into the model every 6 h over a 72-h period and updated as new data become available (NOAA/NHC 2008). This is achieved to a large extent with the use of remotely sensed data. The remote sensing systems used to provide near–realtime data for the models, include geostationary satellites (GOES), which sit above a fixed point on the equator at an altitude of 36,000 km and can provide estimates of the location, size, and intensity of a storm with their visible and thermal infrared imagers over large areas at a spatial resolution of 4 km

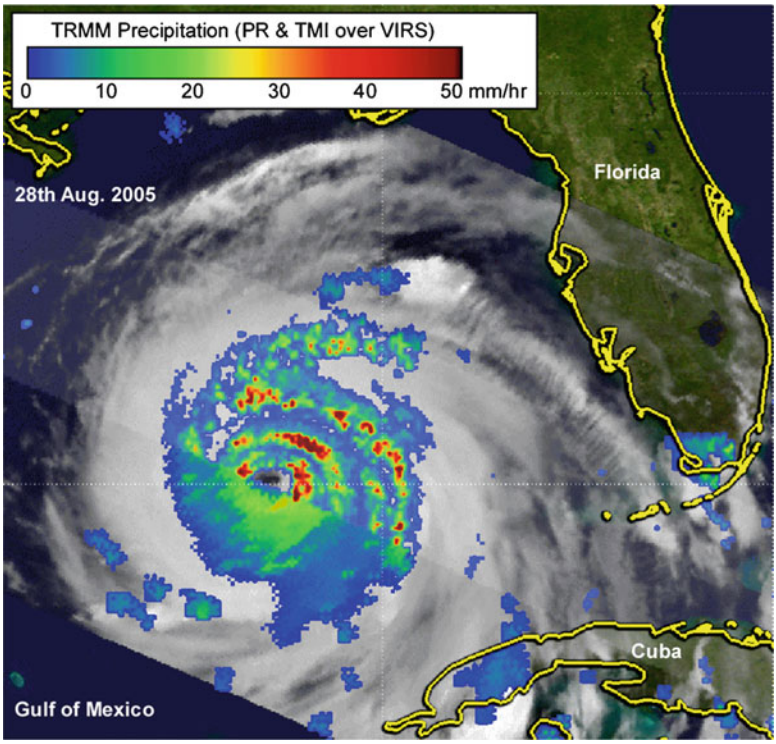

Fig. 2.1 Satellite image of Hurricane Katrina as it passes over the Gulf of Mexico. The image was taken on August 28, 2005, when Katrina had sustained winds of 185 km/h and was becoming a Category 4 hurricane in the central Gulf of Mexico (Credits: NASA 2005)

(NOAA 2006). In the visible region, clouds appear white because they scatter and reflect the sunlight. In thermal infrared images, clouds appear in varying shades of grey, depending on their temperature, which is determined by their height above the Earth. Because geostationary satellites permanently view the same part of the globe, they can provide this information at very frequent intervals (*e.g.,* every 15 min). These images can be supplemented by daily passes of the polar-orbiting NOAA Advanced Very High Resolution Radiometer (AVHRR) sensor, providing a resolution of 1.1 km.

Figure 2.1 shows a satellite image of Hurricane Katrina as it passes over the Gulf of Mexico. The image was enhanced with the use of data from several sensors, including the Tropical Rainfall Measurement Mission (TRMM) satellite and its microwave imager (TMI). By measuring the microwave energy emitted by the Earth and its atmosphere, TMI is able to quantify the water vapor, cloud water, and rainfall intensity in the atmosphere. The image in Fig. 2.1 was taken on August 28, 2005, when Katrina had sustained winds of 185 km/h and was about to become a Category 4 hurricane in the central Gulf of Mexico. The image reveals the horizontal distribution of rain intensity within the hurricane as obtained from TRMM sensors.

Table 2.1 Space-borne ocean sensing techniques

Color scanner	Ocean color (chlorophyll conc., susp. sediment, atten. coeff.)
Infrared radiometer	Sea surface temperature (surface temperature, current patterns)
Synthetic aperture radar	Short surface waves (swell, internal waves, oil slicks, etc.)
Altimeter	Topography and roughness of sea surface (sea level, currents, wave height)
Scatterometer	Amplitude of short surface waves (surface wind velocity, roughness)
Microwave radiometer	Microwave brightness temperature (salinity, surface temp., water vapor, soil moisture)

Rain rates in the central portion of the swath are from the TRMM precipitation radar (PR). The PR is able to provide fine-resolution rainfall data and details on the storm's vertical structure. Rain rates in the outer swath are from the TMI. The rain rates were overlaid on infrared data from the TRMM visible infrared scanner (VIRS). TRMM reveals that Katrina had a closed eye surrounded by concentric rings of heavy rain (red areas) that were associated with outer rain bands. The intense rain near the core of the storm indicates where heat, known as latent heat, is being released into the storm (NASA 2005; Pierce and Lang 2005).

Satellite radar systems can provide additional data on sea surface height, surface currents, surface winds, and wave fields. As shown in Table 2.1, radar satellites can measure wave and sea surface height and currents with altimeters, sea surface winds with scatterometers, and wave fields and other surface features, such as oil slicks, with Synthetic Aperture Radar (SAR) (Ikeda and Dobson 1995; Martin 2004). Satellite microwave radiometers have been used to estimate precipitation amounts and other hydrologic parameters for recent hurricanes like Katrina (Parkinson 2003). Sea surface salinity and soil moisture can also be mapped with microwave radiometers. Table 2.1 includes satellite systems for mapping ocean color (productivity) and sea surface temperature as well.

The International Charter "Space and Major Disasters" (the Charter) has been one of the primary sources of satellite data for the past 11 years to cover events like floods, fires, tsunamis, ocean storms, earthquakes, volcanic eruptions and oil spills. The Charter is a multi-satellite operational system to provide space-borne data on disasters that may have the potential of causing significant loss of life or property (Mahmood 2012). The idea of the Charter as a mechanism to supply satellite data-derived information in situations of crisis was introduced by the European (ESA) and the French (CNES) space agencies in 1999 (Bessis et al. 2003). Once the Canadian Space Agency came on board, the three founding members established the necessary infrastructure to implement the Charter. Since its inception, the Charter membership has grown to 14. The increasing number of satellites and sensors has resulted in a rapid response through shorter revisit frequencies and better recognition of targets with improved spectral and spatial resolutions. The Charter data are delivered to users with fast turn-around times and at no cost. Typically, satellite data are analyzed for change detection by merging the newly acquired, post-disaster imagery with reference imagery retrieved from the archives. The resulting products include maps and geocoded image overlays showing flooded surfaces and

derived water depths, lava flows, impacted roads and bridges, hot spots, burnt areas, and landslide scars. The increasing number of satellites and sensors has resulted in a rapid response through shorter revisit frequencies and better recognition of targets with the improved spectral and spatial resolutions. The Charter data are delivered to users with fast turn-around times and at no cost (Mahmood 2012).

Along the coast, ground-based radars, such as the X-band marine navigation radars, can monitor waves, storm surges, and fronts over a 10-km range with 50-m resolution. Shore-based high-frequency (HF) radars have a range of up to 200 km, but with a resolution of hundreds of meters. HF radars can measure current speeds and wave height and direction. Because shore-based radars are stationary, they can sample frequently and continuously, thus complementing satellite radar data (Cracknell and Hayes 2007; Robinson 2004).

2.3 Assessing Storm Damage to Coastal Ecosystems

Coastal wetlands are a highly productive and critical habitat for a number of plants, fish, shellfish, and other wildlife. Wetlands also provide flood protection, protection from storm and wave damage, water quality improvement through filtering of agricultural and industrial waste, and recharge of aquifers (Morris et al. 2002; Odum 1993). The strong winds, storm surges and heavy rainfall produced by hurricanes in the past have damaged wetland and coral reef ecosystems, especially along the Gulf Coast (Edmiston et al. 2008; Farris 2005).

In southeastern Louisiana, Hurricane Katrina transformed nearly 100 mile^2 (260 km^2) of marsh into open water. Most of the loss east of the Mississippi River was attributed to the effects of Katrina's storm surge. Vegetation was ripped out and sand washed in, scouring and damaging mangrove roots and harming the animals that live there. Large influxes of eroded sediment reduced habitat for coastal birds, mammals, and invertebrate species. Barrier islands were submerged and eroded. Entire seagrass beds, which are critical to fish, sea turtles, and marine mammals, were uprooted and destroyed during the storm. Coral reef beds were scoured, torn, and flattened, causing population reductions in animals such as sea urchins, snails, and fish. Katrina inundated marshes and swamps with saltwater and polluted runoff from urban areas and oil refineries, affecting amphibians and reptiles because of their sensitivity to toxins and other pollutants. Large areas of wetlands were lost, some of them permanently (Barras 2006; Provencher 2007).

The resulting wetland losses caused by Katrina were mapped by NASA, NOAA, and USGS scientists over large areas using medium-resolution satellite imagery and GIS. Time series of Landsat TM, MODIS (Moderate-resolution Imaging Spectroradiometer), and other sensors were used not only to observe the immediate damage to wetlands and forests, but also to monitor their recovery. The satellite images demonstrated how coastal wetlands function to protect inland regions and coastal communities from storm surges unleashed by powerful hurricanes. The wetlands act as a sponge, soaking up water and diminishing the storm surge. If the wetlands

Fig. 2.2 The MODIS Spectroradiometer on NASA's Terra satellite captured this image 13 days after Hurricane Ike came ashore. The *brown* areas in the image are the result of a massive storm surge that Ike pushed far inland over Texas and Louisiana causing a major marsh dieback. Credits: NASA/GSFC

had not been there, the storm surge could have penetrated much farther inland. By contrast, no wetlands existed to buffer New Orleans from Lake Pontchartrain; therefore, the storm forced lake water to burst through the levees that separated it from the city (NASA 2005; NOAA,2008; Stone and Muller 2005).

The value of satellite imagery is illustrated in Fig. 2.2, which shows an image of the Texas coast captured by the MODIS sensor on NASA's Terra satellite 13 days after Hurricane Ike made landfall on September 13, 2008. The storm's surge covered hundreds of kilometers of the Gulf Coast because Ike was a large storm, with tropical-storm-strength winds stretching more than 400 km from the center of the storm. Most of the shoreline in this region is coastal wetland. One can clearly distinguish the brown areas in the image which are the result of the massive storm surge that Ike had pushed far inland over Texas and Louisiana, causing a major marsh dieback. The salty water burned the plants, leaving them wilted and brown. The brown line corresponds with the location and extent of the wetlands. North of the brown line, the vegetation gradually transitions to pale green farmland and dark green natural vegetation untouched by the storm's surge. The powerful tug of water returning to the Gulf also stripped marsh vegetation and soil off the land. Therefore, some of the brown seen in the wetlands may be deposited sediment. Plumes of brown water are visible as sediment-laden water drains from rivers and the coast in general. The muddy water slowly diffuses, turning pale green, green,

and finally blue as it blends with clearer Gulf water. (NASA/GSFC 2010; Ramsey and Rangoonwala 2005).

Traditionally the Landsat Thematic Mapper (TM) and the French SPOT satellite have been reliable sources for land cover and wetland data. Their 30 and 20 m respective spatial resolutions and spectral bands have proven cost-effective for mapping land cover changes in large coastal watersheds (Akumu et al. 2010; Houhoulis and Michener 2000; Jensen 1996; Jensen et al. 1993; Lunetta and Balogh 1999; Porter et al. 2006). However, coastal wetlands and small watersheds frequently require higher resolution data, as provided by aircraft and high-resolution satellite sensors (Adam et al. 2010; Klemas 2011a). As shown in Table 2.2, high resolution imagery (0.6–4 m) can now be obtained from satellites, such as IKONOS and QuickBird. However, cost becomes excessive if the site is larger than a few hundred square kilometers, and in that case, medium resolution sensors, such as Landsat TM (30 m) and SPOT (20 m), become more cost-effective.

A number of advanced new techniques have been developed for mapping wetlands and even identifying wetland types and plant species (Jensen et al. 2007; Klemas 2011a; Schmidt et al. 2004; Yang et al. 2009). For instance, using LiDAR, hyperspectral and radar imagery, and narrow-band vegetation indices, researchers have been able not only discriminate some wetland species, but also make progress on estimating biochemical and biophysical parameters of wetland vegetation, such as water content, biomass and leaf area index (Adam et al. 2010; Gilmore et al. 2010; Ozesmi and Bauer 2002; Schmid et al. 2011; Pengra et al. 2007; Simard et al. 2010; Wang 2010). The integration of hyperspectral imagery and LiDAR-derived elevation data has also significantly improved the accuracy of mapping salt marsh vegetation. The hyperspectral images help distinguish high marsh from other salt marsh communities due to its high reflectance in the near-infrared region of the spectrum, and the LiDAR data help separate invasive *Phragmites* from low marsh plants (Yang and Artigas 2010).

Submerged aquatic plants and their properties are not as easily detectable as terrestrial vegetation. The spectral response of aquatic vegetation resembles that of terrestrial vegetation, yet the submerged or flooded conditions introduce factors that alter its overall spectral characteristics. It is therefore useful to distinguish between submerged and emergent wetland plants, since these factors affect each of them differently. Thus the main challenge for remote sensing of submerged aquatic plants is to isolate the plant signal from the interference of the water column, the bottom and the atmosphere. Furthermore, mapping submerged aquatic vegetation (SAV) and coral reefs requires high-resolution (1–4 m) imagery (Mumby and Edwards 2002; Purkis 2005; Thompson and Schroeder 2010; Trembanis et al. 2008). Coral reef ecosystems usually exist in clear water and their images can be classified to show different forms of coral reef, dead coral, coral rubble, algal cover, sand lagoons and different densities of sea grasses, etc. However, SAV may grow in more turbid waters and thus is more difficult to map. High-resolution (e.g. IKONOS) multispectral imagers have been used to map eelgrass and coral reefs. Hyperspectral imagers improve the results significantly by being able to identify more estuarine and intertidal habitat classes (Garono et al. 2004; Maeder et al. 2002; Mishra et al.

Table 2.2 High-resolution satellite parameters and spectral bands (DigitalGlobe 2003; Orbimage 2003; Parkinson 2003; Space Imaging 2003)

		IKONOS	QuickBird	OrbView-3	WorldView-1	GeoEye-1	WorldView-2
Sponsor		Space imaging	DigitalGlobe	Orbimage	DigitalGlobe	GeoEye	DigitalGlobe
Launched		Sept. 1999	Oct. 2001	June 2003	Sept. 2007	Sept. 2008	Oct. 2009
Spatial resolution (m)	Panchromatic	1.0	0.61	1.0	0.5	0.41	0.5
	Multispectral	4.0	2.44	4.0	n/a	1.65	2
Spectral range (nm)	Panchromatic	525–928	450–900	450–900	400–900	450–800	450–800
	Coastal blue	n/a	n/a	n/a	n/a	n/a	400–450
	Blue	450–520	450–520	450–520	n/a	450–510	450–510
	Green	510–600	520–600	520–600	n/a	510–580	510–580
	Yellow	n/a	n/a	n/a	n/a	n/a	585–625
	Red	630–690	630–690	625–695	n/a	655–690	630–690
	Red edge	n/a	n/a	n/a	n/a	n/a	705–745

2006; Nayegandhi and Brock 2008; Philpot et al. 2004; Wang and Philpot 2007). Airborne LiDARS have also been used with multispectral or hyperspectral imagers to map coral reefs and SAV (Brock and Purkis 2009; Brock et al. 2004, 2006; Palaseanu-Lovejoy et al. 2009; Yang 2009).

The major advantage of airborne remote sensing is that users can define the deployment and characteristics of the remote sensing system. By choosing the appropriate flight altitude and focal length, they can control the spatial resolution and coverage. Furthermore, the user can choose suitable atmospheric (i.e., cloud-free), sun angle and tidal (i.e., low water) conditions (Clark et al. 1997; Myers and Miller 2005). A wide range of multispectral and hyperspectral imagers can be deployed on aircraft. Airborne geo-referenced digital cameras, providing color and color infrared digital imagery are particularly suitable for accurate mapping or interpreting satellite data. Most digital cameras are capable of recording reflected visible to near-infrared light.

2.4 Measuring Beach Profile Changes

Information on beach profiles and coastal bathymetry is important for studies of near-shore geomorphology, hydrology and sedimentary processes. In order to plan sustainable coastal development and implement effective beach erosion control, flood zone delineation and ecosystem protection, coastal managers and scientists need information on long-term and short-term changes taking place along the coast, including changes in beach profiles due to erosion by storms and littoral drift, wetlands changes due to inundation, *etc*. (Finkl 1996; Gesch 2009; Klemas 2011b).

LiDAR techniques, combined with Global Positioning Systems (GPS), make it possible to obtain accurate topographical and bathymetric maps, including shoreline positions (Lillycrop et al. 1997, 2002; West et al. 2001). LiDAR surveys can produce a 10–15 cm vertical accuracy at a spatial resolution greater than one elevation measurement per square meter. This meets the requirements of many coastal research and management applications of LiDAR, including flood zone delineation, monitoring beach nourishment projects, and mapping changes along sandy coasts and shallow benthic environments due to storms or long-term sedimentary processes (Brock and Purkis 2009; Finkl and Andrews 2008; Finkl et al. 2005; Myers and Miller 2005; Pastol 2011). Airborne LiDARs have also been applied with hyperspectral imagers to map wetlands, beaches, coral reefs and SAV (Zawada and Brock 2009).

A LiDAR aircraft mapping configuration usually includes a light aircraft equipped with a LiDAR instrument and GPS, which is operated in tandem with a GPS base station. A typical beach profiling procedure using LiDAR may include cross-shore profiles every 10 m. In coastal applications, the aircraft flies along the coast at heights of about 300–1,000 m, surveying a ground swath directly below the aircraft. The aircraft position throughout the flight is recorded by an onboard

Table 2.3 Typical LiDAR flight parameters

Flying height	300–1,000 m
Vertical accuracy	±15 cm
Horizontal accuracy	DGPS = 3 m; KGPS = 1 m
Maximum depth	50 m (clear water)
Typical *kd* product	4
Coastal *k*	0.2–0.8 (d = 5–20 m)
Estuarine *k*	1.0–4.0 (d = 1–4 m)
Sounding density	3–15 m
Sun angle	18°–25° (to minimize glare)
Scan geometry	Circular (220 m swath)
Sea state	Low (0–1 Beaufort scale)
Water penetration	Green LiDAR (532 nm) used
Aircraft height	Infrared LiDAR (1,064 nm) used

DGPS differential GPS mode, *KGPS* kinematic GPS mode

GPS receiver. The aircraft GPS signals are later combined with signals concurrently collected by a nearby GPS base station. Differential kinematic GPS post-processing determines the aircraft flight trajectory to within about 5 cm (Cracknell and Hayes 2007; Stockdon et al. 2002; Wang 2010).

In LiDAR bathymetry, a laser transmitter/receiver mounted on an aircraft transmits a pulse that travels to the air-water interface, where a portion of this energy reflects back to the receiver. The remaining energy propagates through the water column and reflects off the sea bottom. Since the velocity of the light pulse is known, the water depth can be calculated from the time lapse between the surface return and the bottom return. To maximize water penetration, bathymetric LiDARs employ a blue-green laser with a typical wavelength of 530 nm to range the distance to the seabed.

Laser depth sounding techniques have proven most effective in moderately clear, shallow waters. Typical flight parameters for airborne LiDARs used in bathymetry are shown in Table 2.3. As shown in Table 2.3, the LiDAR system must have a *kd* factor large enough to accommodate the water depth and water turbidity at the study site (k = attenuation coefficient; d = max. water penetration depth). For instance, if a given LiDAR system has a $kd = 4$ and the turbid water has an attenuation coefficient of $k = 1$, the system will be effective only to depths of approximately 4 m. Optical water clarity is the most limiting factor for LiDAR depth detection, so it is important to conduct the LiDAR overflights during tidal and current conditions that minimize the water turbidity due to sediment re-suspension and river inflow (Sinclair 2008). Typically, a LiDAR sensor may collect data down to depths of about three times the Secchi (visible) depth (Estep et al. 1994; Sinclair 1999). Beyond that depth, acoustic (sonar) echo-sounding techniques are used (Brock and Sallenger 2000).

There are various sonar systems available. Echo-sounding profilers, which measure water depth and changes in bottom topography, send out pulses of acoustic energy beneath the boat or other platform. The acoustic "ping" is reflected off the bottom and submerged objects, and recorded by the transceiver. The depth to target

calculation is based on how long it took the reflected pulse to return to the surface and the speed of sound in water under prevailing environmental conditions. The earliest sounders used single beams, but the newer systems use multiple beams, with a large array of beams measuring bottom depths across a wide swath (Bergeron et al. 2007; Cracknell and Hayes 2007). Acoustic backscatter has also been studied in conjunction with Lidar-derived topographic data and habitat classifications in coral reef environments (Foster et al. 2009).

Side-scan imaging sonars emit acoustic pulses in the form of a very wide fan-shaped beam to both sides and at right angles to the track, to produce an image of the seabottom from the backscattered acoustic energy. Sonar echo-sounders and side-scan sonars are frequently housed in a torpedo-shaped "fish", which is towed by cable behind the survey ship at a predetermined height off the bottom (Pittenger, 1989; Thompson and Schroeder 2010). More recently various acoustic sensors have been housed in Remotely Controlled Vehicles (ROVs) or Autonomous Underwater Vehicles (AUV's) (Chadwick 2010).

2.5 Tracking Coastal Currents

Ocean currents influence the global heat transport; weather and climate; larval transport; drift of water pollutants; sediment transport; and marine transportation. Ocean currents are also important to the distribution of the ocean's sea life. Many species of fish rely on currents to move them to breeding grounds, areas with more abundant prey and more suitable water. Knowledge of the current and wave conditions is essential to ships and shipping companies in order to reduce shipping costs, fuel consumption, avoid powerful storms and disasters. Since currents influence so many marine-related activities and processes, meteorologist, oceanographers, ship captains, coastal and fisheries managers, and marine-related agencies need to have up-to-date information on ocean and coastal currents (Briney 2009; Pinet 2009; Purkis and Klemas 2011; Santos 2000).

Satellite remote sensors can determine currents synoptically over extensive ocean and coastal regions. Satellite altimetry is one of the essential remote sensing techniques for monitoring dynamic ocean conditions, including surface currents, local wind speed, and significant wave height. Satellite altimetry measures sea surface heights providing data on geostrophic circulation, including major ocean currents. Ocean currents can also be determined by satellite SAR or tracking the movement of natural thermal and color features in the ocean. The flow patterns of currents like the Gulf Stream are often mapped with satellite thermal infrared scanners (Andersen 1995; Breaker et al. 1994; Canton-Garbin 2008; Clemente-Colon and Pichel 2006; Ducet et al. 2000; Han 2005; Kuo and Yan 1994; Ray and Cartwright 2001; Robinson 2004; Romeiser 2007; Yan and Breaker 1993).

Along the coast and in bays there are local currents generated by tides, winds, storms, and waves. These currents are important for predicting and tracking local disasters, such as coastal flooding, harmful algal blooms, pollutant dispersion, and

sediment transport. Arrays of current meters, ocean drifters and shore-based radar can provide current measurements at local scales. In-situ current sensors can be used to validate remote sensing measurements of currents and to obtain current data at various depths. Coastal engineers distinguish been two basic approaches to coastal and offshore current measurements, the Eulerian and the Lagrangian methods (Morang and Gorman 2005). Eulerian techniques measure the velocity of water flow past a point in the ocean. Lagrangian techniques measure the movement of a parcel of water in the ocean by tracking the position of surface and subsurface drifters or chemical tracers.

The Eulerian method usually involves current meters on buoy moorings which are fixed to the ocean floor and measure currents at various depths, yet only at one specific site. Arrays of such buoy moorings with current meters at various depths are deployed in coastal waters to measure currents at specific sites, such as in tidal inlets or harbor entrance channels. Impeller (propeller) current meters are pointed into the current by a vane, just like moving air orients a wind vane. Current speed is measured by an impeller that is rotated by the force of the current. Thus its rotational velocity is related to the current speed. Acoustic systems, such as Acoustic Doppler Current Profilers (ADCP) and Acoustic Doppler current meters, are more expensive, but can be used in areas where heavy ship traffic or storms might damage impeller current meter moorings (Aanderaa 2004; Davidson-Arnott 2005; InterOcean 2007; Pinet 2009).

Lagrangian ocean drifters are specifically designed to track the movement of water (currents) at various depths. A typical design of such Lagrangian Drifters includes a float or surface buoy connected by a cable to a current drogue. The drogue, set for a specific depth, acts like an underwater sail as it is pushed by the ocean current. The surface float provides buoyancy, contains the electronics and transmits data to satellites. Satellites, ships or coastal tracking stations determine the drifter's position from its transmission signal and relay the data to ground stations, where drift is calculated from the observed positions (Fratantoni 2001; Jenkins 1992; Richardson 1991; Uchida and Imawaki 2003).

Over the past three decades shore-based high frequency (HF) and microwave Doppler radar systems have been deployed to map currents and determine swell-wave parameters along the world's coasts with considerable accuracy. HF radars operate in the 3–30 MHz frequency range and use a ground-wave propagation mode of the electromagnetic waves (Barrick et al. 1977; Bathgate et al. 2006; Essen et al. 2000; Graber et al. 1997; Gurgel et al. 2003; Gurgel and Schlick 2008; Haus et al. 1997; Paduan and Cook 1997; Schofield et al. 2008). The radar surface current measurements use the concept of Bragg scattering from a slightly rough sea surface, modulated by Doppler velocities of the surface currents. When a radar signal hits an ocean wave it usually scatters in many directions. However, when the radar signal scatters off a wave that has a wavelength half of the transmitted signal wavelength, Bragg scattering will return the signal directly to its source, resulting in a very strong received signal. Extraction of swell direction, height, period and current velocity from HF radar data is based on the modulation imposed upon the short

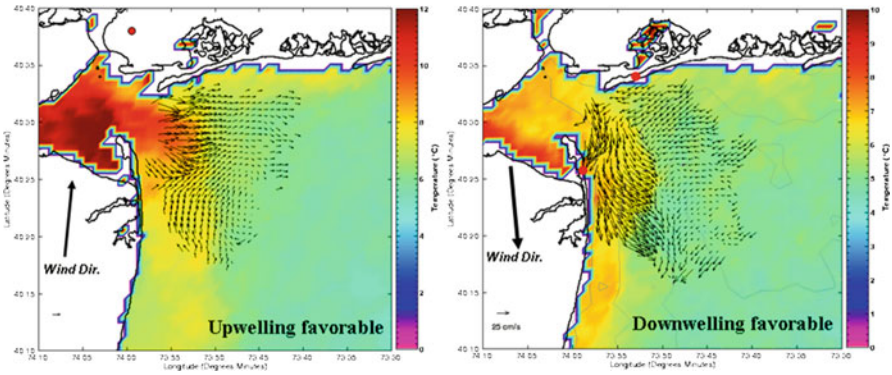

Fig. 2.3 New York Bight surface currents as measured with shore-based HF radar (Courtesy of Coastal Ocean Observation Laboratory, Rutgers University)

Bragg wavelets by the longer faster moving swell (Gurgel et al. 1999; Paduan and Graber 1997; Plant and Keller 1990; Teague et al. 1997).

Surface currents in the New York Bight, as measured with shore-based HF radar for upwelling and downwelling favourable conditions, are shown in Fig. 2.3. This figure also demonstrates how integration of HF data with satellite imagery provides a more complete picture of sea surface dynamics.

Depending on the operating frequency selected, HF radars can attain working ranges of up to 200 km and spatial resolutions between 300 and 1,000 m. Since they can perform continuous measurements, *e.g.* at 10 min intervals, HF radars satisfy the high temporal resolution requirements for tracking tidal and wind-driven currents required for pollution monitoring, ship guidance, rescue operations, and coastal management (Georges et al. 1998; Gurgel et al. 1999; Paduan and Graber 1997; Shearman and Moorhead 1988). Surface current fields have been mapped successfully not only with shore-based, but also with shipborne HF radars (Gurgel 1997; Skop and Peters 1997). Rapid-response HF radar units, such as the SeaSonde, are even being deployed from helicopters to map currents along coastlines in order to improve the modeling and operational prediction of oil slick drift (Kjelaas and Whelan 2011; Paduan and Rosenfeld 1996).

While HF radar provides accurate maps of surface currents and wave information for large coastal areas, their spatial resolution, from hundreds of meters to kilometers, is more suitable for measuring mesoscale features than small-scale currents (Kosro et al. 1997; Romeiser 2007). On the other hand, microwave X-band and S-band radars have resolutions of the order of 10 m, yet have a range of only a few kilometers (Braun et al. 2008; Helzel et al. 2011; Wu et al. 2010). Microwave radars are being used to remotely sense ocean waves and currents close to shore. A new X-band marine radar family (coherent and noncoherent) operating at 10 m scales can measure ocean currents and wave spectra at distances out to a few kilometers (Trizna 2007). Marine radars are also used for tracking coastlines, detecting fixed harbor objects, and other ships, especially in low visibility coastal

fog to avoid collisions. All remote sensing radars, including satellite-borne systems, have the advantage of no instrumentation moored in the open sea, where the instruments may be damaged or lost to storms and ships passing by (Gurgel and Schlick 2008).

2.6 Oil Spill Detection and Tracking

Oil spills can destroy marine life as well as wetland and estuarine animal habitat. To limit the damage by a spill and facilitate containment and cleanup efforts, the shipping operators, oil companies and other responsible agencies must rapidly obtain information on spill location, size and extent of the spill, direction and speed of oil movement, and wind, current and wave information for predicting future oil drift and dispersion. Users of remotely sensed data for oil spill tracking include the Coast Guard, environmental protection agencies, oil companies, shipping/insurance/fishing industries and defense departments (Jha et al. 2008).

Most of the large oil spills in the oceans stem from tanker groundings, break-ups, and collisions resulting in a large fraction of the oil spreading along the surface of the ocean and endangering marine and coastal ecosystems. They are also caused by tankers releasing their ballast water. In most of these cases a wide range of remote sensors have provided the required data for tracking and predicting the future movement of the spilled oil in a timely and reliable manner, helping guide rescue and defensive efforts, including the deployment of skimming vessels and protective booms (DeAngelo 2008; Harris 1997; Klemas 2010).

For oil spill emergencies the main operational data requirements are fast turn-around time and frequent imaging of the site to monitor the dynamics of the spill. Remote sensors on satellites and aircraft meet these requirements by tracking the spilled oil at various resolutions and over wide areas at frequent intervals through multi-temporal imaging. They also provide key inputs to drift prediction models and facilitate targeting of clean-up and control efforts (Brecke and Solberg 2005; Fingas 2010).

There are various models being used to predict the drift and dispersion of oil spilled in the ocean. One such model is the general NOAA Operational Modeling Environment (GNOME) oil spill trajectory model used by the NOAA National Ocean Service's Emergency Response Division (ERD). GNOME is used by ERD in a diagnostic mode to set up custom scenarios quickly. It is also available in a Standard Mode to outside users to predict how wind, currents and other processes might move and spread the spilled oil; learn how predicted oil trajectories are affected by uncertainties in current and wind observations and forecasts; and see how spilled oil is predicted to "weather". After entering information on an oil spill scenario, GNOME displays the trajectory of the oil. (NOAA/ERD 2010).

Most of the remote sensors use electromagnetic waves, even though acoustic sensors on boats and cameras on submerged robot-like vehicles may have to be used to view the subsurface behavior of the oil (Brecke and Solberg 2005; Jha et al. 2008;

Fig. 2.4 Deepwater Horizon oil spill captured on April 29, 2010 by MODIS imager on NASA's Terra satellite. Credits: NASA Goddard Space Flight Center

NOAA/ERD 2010; UCAR 2010). Table 2.4 summarizes the various ways of detecting oil slicks on water using electromagnetic waves. In the ultraviolet region oil fluoresces and thus appears to have a significantly higher reflectivity than water, even for very thin slicks. However, ultraviolet light is strongly scattered by the atmosphere and, in order to avoid such scattering, can be used only on aircraft at low altitudes.

Visible wavelengths are used more commonly due to the availability of relatively inexpensive digital cameras on aircraft and multispectral imagers on satellites. There is also a reasonable atmospheric transmission window for visible wavelengths. In the visible region oil has a slightly higher reflectivity than water. Oil sheen shows up as silvery and reflects light over a wide spectral region. Heavy oil appears brown, peaking in the 600–700 nm region, while mousse looks red-brown and peaks closer to 700 nm. In Fig. 2.4, the MODIS image of the Deepwater Horizon oil spill in the Gulf of Mexico clearly shows the silvery oil slick to the right of the Mississippi Delta. Sunglint and oil sheen help enhance the appearance of the slick.

Improvements in sensor technology have led to the development of hyperspectral sensors, such as the Airborne Visible/Infrared Spectrometer (AVIRIS) and the Airborne Imaging Spectrometer (AISA). A hyperspectral image consists of tens to hundreds of spectral bands and can provide a detailed spectral identification of a

feature, such as differentiating between light and crude oil and detecting small concentrations of oil (Brecke and Solberg 2005; Jensen 2007).

At thermal infrared wavelengths "optically thick" oil layers absorb solar radiation and re-emit it as thermal energy in the 8–14 μm region. Thin oil slicks or sheen cannot be detected by thermal infrared sensors. However, layers thicker than about 150 μm appear hot or bright, while layers less than about 50 μm appear cool and dark. This variability in apparent temperature may help distinguish thick layers of oil from thin layers, yet it also can cause interpreters to have difficulty distinguishing oil from water (Jha et al. 2008).

Radar imagers such as Side-Looking Airborne Radar (SLAR) on aircraft and Synthetic Aperture Radar (SAR) on satellites have the major advantage of not being bothered by cloud cover and other atmospheric effects, which frequently eliminate visible and infrared wavelengths from contention (Table 2.4). Features found frequently in SAR data are regions of low backscatter caused by the presence of oil or other slicks on the sea-surface. SAR imagers view the ocean surface at incidence angles between approximately 20° and 30° from the local vertical. Capillary waves and short gravity waves cause the radar pulse to be scattered, including some backscattering to the radar transmitter. As short surface gravity waves or capillary ripples propagate through a region where an oil film is present, their energy is absorbed as the surface film strains, causing damping of these short waves. The film-covered area backscatters less energy to the radar receiver, since most of the radar pulse is reflected from the flatter surface in the opposite direction. Thus ocean surface areas covered by oil or other slicks show up as dark in radar images. For this to work, low to moderate winds must exist to create the short surface waves. (Brecke and Solberg 2005; Fingas 2010; Harris 1997; Jha et al. 2008; Robinson 2004).

2.7 Mapping Algal Blooms

High concentrations of nutrients from agricultural and urban run-off, or produced by coastal upwelling, are causing algal blooms in many estuaries and coastal waters. Algal blooms induce eutrophic conditions, depleting oxygen levels needed by organic life, limiting aquatic plant growth by reducing water transparency, and producing toxins which can harm fish, benthic animals and humans, and are often referred to as Hazardous Algal Blooms (HAB). The frequency of algal blooms and associated problems, like eutrophication, are increasing in many estuarine and coastal waters because of the effects from increased nutrient loads from urban and agricultural run-off (Boesch et al. 2009; Kennish 2002; Kennish and Townsend 2007; Smith 2006; Yang 2009). The triggers for bloom conditions are not fully understood, but nutrient enrichment of waters, especially by nitrogen and/or phosphates, as well as unusually warm conditions, are recognized as precursors. With such diverse causes, prevention of HABs is difficult. Therefore, a more efficient means of dealing with this threat is through an effective early warning

Table 2.4 Applicability of electromagnetic wave bands for oil detection

EM band	Wavelength	Detection mechanism	Contrast vs. water	Thickness	Night operation	Weather limitations	False targets
Ultraviolet	0.3–0.4 μm	Reflectivity oil > water fluorescence	Bright	No	No	Clear	Low Sun-glint, wind sheen
Visible bands	0.4–0.7 μm	Reflectivity oil > water	Bright	No	No	Clear	High Sun-glint, wind sheen
Reflected infrared	0.7–3 μm	Reflectivity oil > water	Bright	No	No	Clear	High Sun-glint, wind sheen
Thermal infrared	3–14 μm	Emissivity Oil > water (>30 μm)	Dark/bright	Relative	Yes Day-warm, night-cool	Light fog	Medium Thin oil vs. cold water (<100 μm)
Radar	1–30 cm	Damped ripples (Wind 2–12 m/s)	Dark	No (Thick oil vs. sheen)	Yes	Heavy fog and rain	High Other films and slicks
Passive microwave	0.2–0.8 cm	Emissivity Oil > water	Bright	Relative	Yes	Heavy fog and rain	Low Biogenic materials

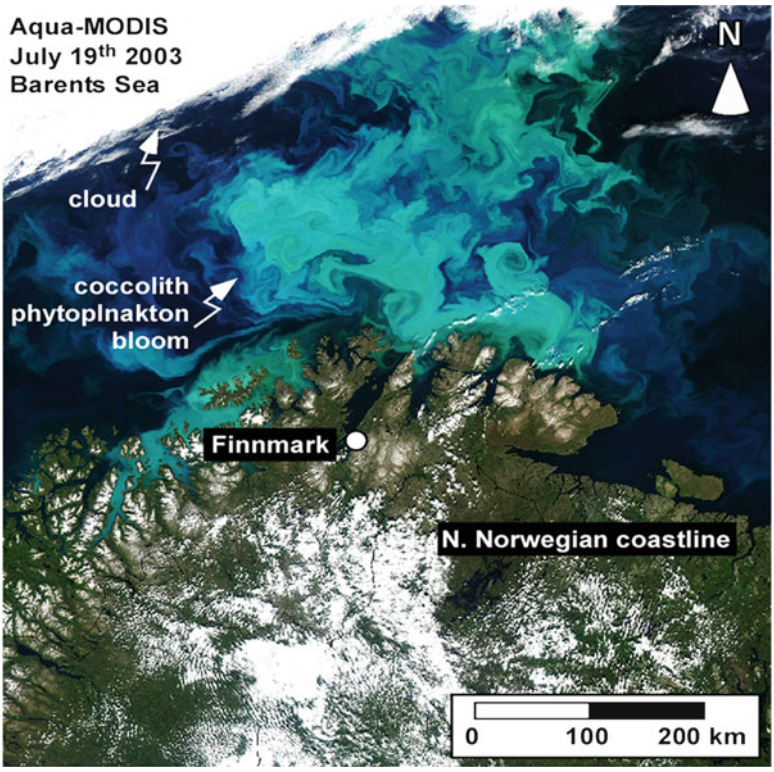

Fig. 2.5 Phytoplankton bloom in the Barents Sea (Arctic Ocean) as seen in Aqua-MODIS imagery on July 19, 2003. The bloom is composed of coccolithophores and covers an area of over 500 km^2 off Finnmark, the most northern and eastern county of Norway. Credit: NASA's Earth Observatory

system based on remotely sensed images of early bloom indicators (Jochens et al. 2010; Stumpf et al. 2009).

Satellite and airborne measurements of spectral reflectance (ocean color) represent an effective way for monitoring phytoplankton by its proxy, chlorophyll-a, the green pigment that is present in all algae. As shown in Fig. 2.5, most algal blooms can be observed with multispectral sensors on satellites because of their distinct color (Klemas 2012; Ruddick 2001; Stumpf and Tomlinson 2005). Furthermore, hyperspectral sensors with spectral bands fine-tuned for specific pigment analysis, allow detection and analysis of algal taxonomy. This can be accomplished because the species-specific algal accessory pigments produce unique spectral signatures. Remote sensing data can complement monitoring networks existing in many parts of the world to obtain data on nutrient loading and algal growth. This gives scientists better insights into overall water quality, distribution of toxin-producing algae and aquatic biogeochemical cycling (Gitelson 1993; Simis 2005).

2.8 Summary and Conclusions

Environmental and economic impacts from coastal storms and other disasters can include beach erosion, wetland destruction, excessive nutrient loading, algal blooms, hypoxia and anoxia, fish kills, large scale releases of pollutants, and spread of pathogens. Over the long term, coastal communities are also facing a rising sea level, caused mainly by global warming. Coastal agencies need advance information on the predicted path, intensity and progress of a storm and associated waves and storm surge; near-real-time information during the peak of the storm to monitor flooding and control rescue operations; and after the storm to assess the damage and plan and implement the recovery. The same holds true for other disasters, such as oil spills and algal blooms. Airborne and satellite remote sensors have helped provide this information, together with observers in aircraft and on the ground.

The Landsat Thematic Mapper (TM) has proven cost-effective for observing land cover changes in large coastal watersheds. Coastal wetlands and small watersheds frequently require higher resolution data, as provided by aircraft. High resolution imagery (0.6–4 m) can now also be obtained from satellites, such as IKONOS and QuickBird. However, cost becomes excessive if the site is larger than a few hundred square kilometers, and in that case, medium resolution sensors, such as Landsat TM (30 m) and SPOT (20 m), become more cost-effective. Wetland species identification is difficult; however, some progress is being made using hyperspectral imagers

In order to plan and implement effective beach erosion control, flood zone delineation and ecosystem protection, coastal managers and scientists need information on long-term and short-term changes taking place along the coast, including changes in beach profiles due to erosion by storms and littoral drift, wetlands changes due to inundation, etc. LiDAR techniques, combined with Global Positioning Systems (GPS), make it possible to obtain accurate topographical and bathymetric maps, including shoreline positions. LiDAR surveys can produce a 10–15 cm vertical accuracy at a spatial resolution greater than one elevation measurement per square meter.

Satellite remote sensors can determine currents synoptically over extensive ocean and coastal regions. Satellite altimetry is one of the essential remote sensing techniques for monitoring dynamic ocean conditions, including surface currents, local wind speed, and significant wave height. Satellite altimetry measures sea surface heights providing data on geostrophic circulation, including major ocean currents. Ocean currents can also be determined by satellite SAR or tracking the movement of natural thermal and color features in the ocean. The flow patterns of currents like the Gulf Stream are often mapped with satellite thermal infrared scanners.

Along the coast and in bays there are local currents generated by tides, winds, storms, and waves. These currents are important for predicting and tracking local disasters, such as coastal flooding, harmful algal blooms, pollutant dispersion, and sediment transport. Over the past three decades shore-based high frequency (HF) and microwave Doppler radar systems have been deployed to map currents and

determine swell-wave parameters along the world's coasts with working ranges of up to 200 km and spatial resolutions between 300 and 1,000 m. Since they can perform continuous measurements, *e.g.* at 10 min intervals, HF radars satisfy the high temporal resolution requirements for tracking tidal and wind-driven currents.

For oil spill emergencies the main operational data requirements are fast turn-around time and frequent imaging of the site to monitor the dynamics of the spill. Remote sensors on satellites and aircraft meet these requirements by tracking the spilled oil at various resolutions and over wide areas at frequent intervals through multi-temporal imaging. They also provide key inputs to drift prediction models and facilitate targeting of clean-up and control efforts.

Algal blooms induce eutrophic conditions, depleting oxygen levels needed by organic life, limiting aquatic plant growth by reducing water transparency, and producing toxins which can harm fish, benthic animals and humans. The frequency of hazardous algal blooms (HABs) and associated eutrophication problems is increasing in many estuarine and coastal waters because of the effects of eutrophication, resulting from increased nutrient loads from urban and agricultural run-off. Satellite and airborne measurements of spectral reflectance (ocean color) represent an effective way for monitoring phytoplankton by its proxy, chlorophyll-a, the green pigment that is present in all algae. Most HABs can be observed with satellite and airborne multispectral sensors because of their distinct color. Furthermore, the spectral bands of hyperspectral sensors can be fine-tuned for specific pigment detection. In sum, it appears that satellite and airborne remote sensors can provide much of the information required for coastal hazard detection and monitoring.

References

Aanderaa (2004) The RCM 9: a recording current meter featuring the Mark II Doppler Current Sensor DCS 3920. Aanderaa Instruments. Data Sheet, D 328, October 2004, pp 1–8

Adam E, Mutanga O, Rugege D (2010) Multispectral and hyperspectral remote sensing for identification and mapping of wetland vegetation: a review. Wetl Ecol Manag 18:281–296

Akumu CE, Pathirana S, Baban S, Bucher D (2010) Monitoring coastal wetland communities in north-eastern NSW using ASTER and Landsat satellite data. Wetl Ecol Manag 18:357–365

Andersen OB (1995) Global ocean tides from ERS-1 and TOPEX/POSEIDON altimetry. J Geophys Res 100:25249–25259

Barras J (2006) Land area change in coastal Louisiana after the 2005 hurricanes – a series of three maps. U.S. geological survey open-file report 06–1274, 12 p

Barrick DE, Evans MW, Weber BL (1977) Ocean surface current mapped by radar. Science 198:138–144

Bathgate J, Heron M, Prytz A (2006) A method of swell parameter extraction from HF ocean surface radar spectra. IEEE J Ocean Eng 31:812–818

Bergeron E, Worley CR, O'Brien T (2007) Progress in the development of shallow water mapping systems. Sea Technol 48:10–16

Bessis JL, Bequignon J, Mahmood A (2003) The international charter "space and major disasters" initiative. Acta Astronaut 54:183–190

Boesch DF, Boynton WR, Crowder LB, Diaz RJ, Howarth RW, Mee LD, Nixon SW, Rabalais NN, Rosenberg R, Sanders JG, Scavia D, Turner RE (2009) Nutrient enrichment drives Gulf of Mexico hypoxia. Am Geophys Union EOS Trans 90:117–118

Braun N, Ziemer F, Bezuglov A, Cysewski M, Schymura G (2008) Sea-surface current features observed by Doppler radar. IEEE Trans Geosci Remote Sens 46:1125–1133

Breaker LC, Krasnopolsky VM, Rao DB, Yan X-H (1994) The feasibility of estimating ocean surface currents on an operational basis using satellite feature tracking methods. Bull Am Meteorol Soc 75:2085–2095

Brecke C, Solberg AHS (2005) Oil spill detection by satellite remote sensing. Remote Sens Environ 95:1–13

Briney A (2009) Ocean currents. About.com. Geography. http://geography.about.com/od/physicalgeography/a/oceancurrents.htm Accessed 29 Nov 2011

Brock JC, Purkis SJ (2009) The emerging role of LiDAR remote sensing in coastal research and resource management. Special Issue 53-Coastal Applications of Airborne LiDAR. J Coast Res 53:1–5

Brock JC, Sallenger A (2000) Airborne topographic mapping for coastal science and resource management. US Geological Survey, Washington, DC, pp 01–46

Brock JC, Wright CW, Clayton TD, Nayegandhi A (2004) LIDAR optical rugosity of coral reefs in Biscayne National Park, Florida. Coral Reef 23:48–59

Brock JC, Wright CW, Hernandez R, Thompson P (2006) Airborne LiDAR sensing of massive stony coral colonies on patch reefs in the northern Florida reef tract. Remote Sens Environ 104:31–42

Canton-Garbin M (2008) Satellite ocean observation in relation to global change. In: Chuvieco E (ed) Earth observation of global change. Springer, Berlin

Chadwick W (2010) Remotely operated vehicles (ROVs) and autonomous underwater vehicles (AUVs). NOAA ocean explorer: submarine ring of fire 2002: background. http://oceanexplorer.noaa.gov/explorations/02fire/background/rovsauvs/rov_auv.html

Clark C, Ripley H, Green E, Edwards A, Mumby P (1997) Mapping and measurement of tropiocal coastal environments with hyperspectral and high spatial resolution data. Int J Remote Sens 18:237–242

Clemente-Colon P, Pichel WG (2006) Remote sensing of marine pollution. In: Gower J (ed) Manual of remote sensing, vol 6, 3rd edn. (A.N.Rencz, Editor-in Chief). American Society of Photogrammetry and Remote Sensing, Washington, DC, ISBN 1-57083-080-0

Cracknell AP, Hayes L (2007) Introduction to remote sensing. CRC Press, New York

Davidson-Arnott R (2005) Beach and near-shore instrumentation. In: Schwartz ML (ed) Encyclopedia of coastal science. Springer, Dordrecht, pp 130–138

DeAngelo L (2008) The sea empress oil spill. http://www.eoearth.org/article/Milford_Haven,_Wales

Digital Globe (2003) Quickbird imagery products and product guide (revision 4). Digital Globe, Inc., Longmont

Ducet N, Le Traon PY, Reverdin G (2000) Global high-resolution mapping of ocean circulation from TOPEX/Poseidon and ERS-1 and -2. J Geophys Res 105:19477–19498

Edmiston HL, Fahrny SA, Lamb MS, Levi LK, Wanat JM, Avant JS, Wren K, Selly NC (2008) Tropical storm and hurricane impacts on a Gulf Coast estuary: Apalachicola Bay, Florida. J Coast Res Spec Issue 55:38–49

Essen HH, Gurgel KW, Schlick T (2000) On the accuracy of current measurements by means of HF radar. IEEE J Ocean Eng 25:472–480

Estep LL, Lillycrop WJ, Parson LE (1994) Estimation of maximumdepth of penetration of a bathymetric lidar system using a Secchi Depth data base. Mar Technol Soc J 28:31–36

Farris GS (2005) USGS reports new Wetland loss from Hurricane Katrina in Southeastern Louisiana. http://www.usgs.gov/newsroom/article. Accessed 13 Mar 2009

Fingas M (2010) Oil spill science and technology. Elsevier, Amsterdam, 1192 pp

Finkl CW (1996) What might happen to America's shorelines if artificial beach replenishment is curtailed: a prognosis for southeastern Florida and other sandy regions along regressive coasts. J Coast Res 12:ii–ix

Finkl CW, Andrews JL (2008) Shelf geomorphology along the Southeast Florida Atlantic continental platform: barrier coral reefs, nearshore bedrock, and morphosedimentary features. J Coast Res 24:823–849

Finkl CW, Benedet L, Andrews JL (2005) Interpretation of seabed geomorphology based on spatial analysis of high-density airborne laser bathymetry (ALB). J Coast Res 21:501–514

Foster G, Walker BK, Riegl BM (2009) Interpretation of single-beam acoustic backscatter using Lidar-derived topographic complexity and benthic habitat classification in a coral reef environment. J Coast Res Spec Issue 53:16–26

Fratantoni DM (2001) North Atlantic surface circulation during the 1990s observed with satellite-tracked drifters. J Geophys Res 106(C10):22067–22094

Garono RJ, Simenstad CA, Robinson R, Ripley H (2004) Using high spatial resolution hyperspectral imagery to map intertidal habitat structure in Hood Canal Washington, USA. Can J Remote Sens 30:54–63

Georges TM, Harlan JA, Lee TN, Leben RR (1998) Observations of the Florida Current with two over-the-horizon radars. Radio Sci 33:1227–1239

Gesch DB (2009) Analysis of Lidar elevation data for improved identification and delineation of lands vulnerable to sea-level rise. J Coast Res Spec Issue, Coast Appl Airborne Lidar 53:49–58

Gilmore MS, Civco DL, Wilson EH, Barrett N, Prisloe S, Hurd JD, Chadwick C (2010) Remote sensing and in situ measurements for delineation and assessment of coastal marshes and their constituent species. In: Wang J (ed) Remote sensing of coastal environment. CRC Press, Boca Raton

Gitelson A (1993) Quantitative remote sensing methods for real-time monitoring of inland water quality. Int J Remote Sens 14:1269–1295

Graber HC, Haus BK, Chapman RD, Shay LK (1997) HF radar comparisons with moored estimates of current speed and direction: expected differences and implications. J Geophys Res 102:18749–18766

Gurgel K-W (1997) Experience with shipborne measurements of surface current fields by radar. Oceanography 10:82–84

Gurgel K-W, Schlick T (2008) Land-based over-the-horizon radar techniques for monitoring the North-East Atlantic Coastal Zone. In: Barale V, Gade M (eds) Remote sensing of the European seas. Springer, Dordrecht, pp 447–458

Gurgel K-W, Essen HH, Kingsley HP (1999) HF radars: physical limitations and recent developments. Coast Eng 37:201–218

Gurgel K-W, Essen HH, Schlick T (2003) The use of HF radar networks within operational forecasting systems of coastal regions. In: Dahlin H, Flemming NC, Nittis K, Petersson SE (eds) Building the European capacity in operational oceanography. Elsevier, Oxford, pp 245–250

Han G (2005) Altimeter surveys, coastal tides and shelf circulation. In: Schwartz ML (ed) Encyclopedia of coastal science. Springer, Dordrecht, pp 27–28

Harris C (1997) The sea empress incident: overview and response at sea. In: Proceedings of the 1997 oil spill conference, Fort Lauderdale, FL, 7–10 April 1997, pp 177–184

Haus BK, Graber HC, Shay LK (1997) Synoptic measurement of dynamic ocean features. Oceanogr: Spec Issue High Freq Radars Coast Oceanogr 10:45–48

Hayes B (2005) Natural and unnatural disasters. Am Sci 93:496–499

Helzel T, Petersen L, Mariette V, Pavec M (2011) Reliability of coastal radar WERA for coastal zone management. J Coast Res Spec Issue 64:1345–1347

Houhoulis PF, Michener WK (2000) Detecting wetland change: a rule-based approach using NWI and SPOT-XS data. Photogramm Eng Remote Sens 66:205–211

Ikeda M, Dobson FW (1995) Oceanographic applications of remote sensing. CRC Press, New York

InterOcean (2007) S4 current meter family. InterOcean Systems, Inc. http://www.interoceansystems.com/s4theory.htm. Accessed 16 March, 2007
IPCC (2007) Intergovernmental panel on climate change. Climate change 2007: the physical science basis. WMO/UNEP, Paris (www.ipcc.ch)
Jenkins WJ (1992) Tracers in oceanography. Oceanus 35:47–55
Jensen JR (1996) Introductory digital image processing: a remote sensing perspective, 2nd edn. Prentice-Hall, Upper Saddle River
Jensen JR (2007) Remote sensing of the environment: an earth resource perspective. Prentice Hall, Upper Saddle River
Jensen JR, Cowen D, Althausen J, Narumalani S, Weatherbee O (1993) An evaluation of the Coast Watch change detection protocol in South Carolina. Photogramm Eng Remote Sens 59:1036–1046
Jensen RR, Mausel P, Dias N, Gonser R, Yang C, Everitt J, Fletcher R (2007) Spectral analysis of coastal vegetation and land cover using AISA + hyperspectral data. Geocarto Int 22:17–28
Jha MN, Levy J, Gao Y (2008) Advances in remote sensing of oil spill disaster management: state-of-the-art sensor technology for oil spill surveillance. Sensors 8:236–255
Jochens TT, Malone TC, Stumpf RP, Hickey BM, Carter M, Morrison R, Dyble J, Jones B, Trainer VL (2010) Integrated ocean observing system in support of forecasting harmful algal blooms. Mar Technol Soc J 44:99–121
Kennish MJ (2002) Environmental threats and environmental future of estuaries. Environ Conserv 29:78–107
Kennish MJ, Townsend AR (2007) Nutrient enrichment and estuarine eutrophication. Ecol Appl 17:S1–S2
Kjelaas AG, Whelan C (2011) Rapidly deployable SeaSonde for modeling oil spill response. Sea Technol 52:10–15
Klemas V (2009) The role of remote sensing in predicting and determining coastal storm impacts. J Coast Res 25:1264–1275
Klemas V (2010) Tracking oil slicks and predicting their trajectories using remote sensors and models: case studies of the Sea Princess and Deepwater Horizon oil spills. J Coast Res 26 (5):789–797
Klemas V (2011a) Remote sensing of wetlands: case studies comparing practical techniques. J Coast Res 27:418–427
Klemas V (2011b) Beach profiling and LIDAR bathymetry: an overview with case studies. J Coast Res 27:1019–1028
Klemas V (2012) Remote sensing of algal blooms: an overview with case studies. J Coast Res 28:34–43
Kosro PM, Barth JA, Strub PT (1997) The coastal jet: observations of surface currents over the Oregon Continental Shelf from HF radar. Oceanogr: Spec Issue High Freq Radars Coast Oceanogr, 10:53–56
Kuo N-J, Yan X-H (1994) Using the shape-matching method to compute sea-surface velocities from AVHRR satellite images. IEEE Trans Geosci Remote Sens 32:724–728
Lillycrop WJ, Irish JL, Parson LE (1997) SHOALS system. Sea Technol 38:17–25
Lillycrop WJ, Pope RW, Wozencraft JM (2002) Airborne lidar hydrography: a vision for tomorrow. Sea Technol 43(6):27–34
Lunetta RS, Balogh ME (1999) Application of multi-temporal Landsat 5 TM imagery for wetland identification. Photogramm Eng Remote Sens 65:1303–1310
Maeder J, Narumalani S, Rundquist D, Perk R, Schalles J, Hutchins K, Keck J (2002) Classifying and mapping general coral-reef structure using Ikonos data. Photogramm Eng Remote Sens 68:1297–1305
Mahmood A (2012) Monitoring disasters with a constellation of satellites – type examples from the International Charter "Space and Major Disasters". Geocarto Int 27:91–102
Martin S (2004) An introduction to remote sensing. Cambridge University Press, Cambridge

Mishra D, Narumalani S, Rundquist D, Lawson M (2006) Benthic habitat mapping in tropical marine environments using QuickBird multispectral data. Photogramm Eng Remote Sens 72:1037–1048
Morang A, Gorman LT (2005) Monitoring coastal geomorphology. In: Schwartz ML (ed) Encyclopedia of coastal science. Springer, Dordrecht, pp 447–458
Morris JT, Sundareshwar PV, Nietch CT, Kjerfve B, Cahoon DR (2002) Responses of coastal wetlands to rising sea level. Ecology 83:2869–2877
Mumby PJ, Edwards AJ (2002) Mapping marine environments with IKONOS imagery: enhanced spatial resolution can deliver greater thematic accuracy. Remote Sens Environ 82:248–257
Myers JS, Miller RL (2005) Optical airborne remote sensing. In: Miller RL, DelCastillo CE, McKee BA (eds) Remote sensing of coastal aquatic environments: technologies, techniques and applications. Springer, Dordrecht, pp 51–68
NASA (2005) EO natural hazards: Hurricane Katrina floods the Southeastern United States. http://earthobservatory.nasa.gov/Natural_ Hazards/natural_hazards_v2. Accessed 2 May 2008
NASA/GSFC (2010) Hurricane Ike: storm surge flooding image of the Gulf Coast. NASA image courtesy Jeff Schmaltz, MODIS Rapid Response Team at NASA GSFC
Nayegandhi A, Brock JC (2008) Assessment of coastal vegetation habitats using LiDAR. In: Yang X (ed) Lecture notes in geoinformation and cartography – remote sensing and geospatial technologies for coastal ecosystem assessment and management. Springer Publications, Heidelberg, pp 365–389
NOAA (National Oceanic and Atmospheric Administration) (1999) Trends in U.S. coastal regions, 1970–1998. In: Addendum to the proceedings: trends, and future challenges for U.S. National Ocean and Coastal Policy, NOAA, Washington, DC, August 1999
NOAA (2006) Hurricanes: unleashing nature's fury. A preparedness guide. U.S. Department of Commerce, NOAA, National Weather Service, Washington, DC, pp 1–24
NOAA (2008) Hurricane Katrina. http://www.katrina.noaa.gov/. Accessed 10 Nov 2008
NOAA/CSC (Coastal Services Center) (2008) Hurricane planning with satellite imagery. http://www.csc.noaa.gov/products/sccoasts/html/hazards/htm. Accessed 19 Nov 2008
NOAA/ERD (2010) General NOAA Operational Modeling Environment (GNOME model). http://response.restoration.noaa.gov
NOAA/NHC (National Hurricane Center) (2008) Hurricane preparedness: SLOSH model. http://www.nhc.noaa.gov/HAW2/surge/slosh.shtml. Accessed 22 Nov 2008
Odum EP (1993) Ecology and our endangered life-support systems, 2nd edn. Sinauer Associates, Inc., Sunderland
Orbimage (2003) OrbView-3 satellite and ground systems specifications. Orbimage Inc., Virginia
Ozesmi SL, Bauer ME (2002) Satellite remote sensing of wetlands. Wetl Ecol Manag 10:381–402
Paduan JD, Cook MS (1997) Mapping surface currents in Monterey Bay with CODAR-type HF radar. Oceanogr: Spec Issue High Freq Radars Coast Oceanogr 10:49–52
Paduan JD, Graber HC (1997) Introduction to high-frequency radar: reality and myth. Oceanogr: Spec Issue High Freq Radars Coast Oceanogr 10:36–39
Paduan JD, Rosenfeld LK (1996) Remotely sensed surface currents in Monterey Bay from shore-based radar (Coastal Ocean Dynamics Application Radar). J Geophys Res 101:20669–20686
Palaseanu-Lovejoy M, Nayegandhi A, Brock J, Woodman R, Wright CW (2009) Evaluation of airborne Lidar data to predict vegetation presence/absence. J Coast Res Spec Issue 53:83–97
Parkinson CL (2003) Aqua: an earth-observing satellite mission to examine water and other climate variables. IEEE Trans Geosci Remote Sens 41:173–183
Pastol Y (2011) Use of airborne LIDAR bathymetry for coastal hydrographic surveying: the French experience. J Coast Res Spec Issue 62:6–18
Pengra BW, Johnston CA, Loveland TR (2007) Mapping an invasive plant, Phragmites australis, in coastal wetlands using the EO-! Hyperion hyperspectral sensor. Remote Sens Environ 108:74–81

Philpot WD, Davis CO, Bissett P, Mobley CD, Kohler DD, Lee Z, Snyder WA, Steward RG, Agrawal Y, Trowbridge J, Gould R, Arnone R (2004) Bottom characterization from hyperspectral image data. Oceanography 17:76–85
Pierce H, Lang S (2005) TRMM – tropical rainfall measurement mission: Katrina intensifies into a powerful hurricane, strikes Northern Gulf Coast. http://trmm.gsfc.nasa.gov/publicationsLdir/katrinaLaug05Lno2.html. Accessed 2 May 2008
Pinet PR (2009) Invitation to oceanography, 5th edn. Jones and Bartlett, Sudbury
Pittenger RF (1989) Exploring and mapping the seafloor. National Geographic 177:61A.
Plant WJ, Keller WC (1990) Evidence of Bragg scattering in microwave Doppler spectra of sea return. J Geophys Res 95:16299–16310
Porter DE, Field DW, Klemas VV, Jensen JR, Malhotra A, Field RT, Walker SP (2006) RESAAP final report: NOAA/NERRS remote sensing applications assessment project. University of South Carolina, Columbia
Provencher J (2007) Stronger storms are bad news for coastal ecosystems. Ocean News 7:2–4
Purkis SJ (2005) A 'reef-up' approach to classifying coral habitats from IKONOS imagery. IEEE Trans Geosci Remote Sens 43:1375–1390
Purkis SJ, Klemas V (2011) Remote sensing and global environmental change. Wiley-Blackwell, Oxford, 384 p
Ramsey E, Rangoonwala A (2005) Leaf optical property changes associated with the occurrence of Spartina alterniflora dieback in coastal Louisiana related to remote sensing mapping. Photogramm Eng Remote Sens 71:299–311
Ray RD, Cartwright DE (2001) Estimates of internal tide energy fluxes from TOPEX/Poseidon altimetry: central North Pacific. Geophys Res Lett 28:1259–1262
Richardson PL (1991) SOFAR floats give a new view off ocean eddies. Oceanus 34:23–31
Robinson IS (2004) Measuring the oceans from space: the principles and methods of satellite oceanography. Springer-Praxis Publishing Ltd., Chichester
Romeiser R (2007) High-resolution imaging of current fields from satellites. Sea Technol September 2007 Spec Issue 53:44–46
Ruddick KG (2001) Optical remote sensing of chlorophyll-a in case 2 waters by use of an adaptive two-band algorithm with optimal error properties. Appl Opt 40:3575–3585
Rykhus RP (2005) Satellite imagery maps Hurricane Katrina induced flooding and oil slicks. Am Geophys Union EOS 86:381–382
Santos AMP (2000) Fisheries oceanography using satellite and airborne remote sensing methods: a review. Fish Res 49:1–20
Schmid KA, Hadley BC, Wijekoon N (2011) Vertical accuracy and use of topographic LIDAR data in coastal marshes. J Coast Res 27:116–132
Schmidt KS, Skidmore AK, Kloosterman EH, Van Oosten H, Kumar L, Janssen JAM (2004) Mapping coastal vegetation using an expert system and hyperspectral imagery. Photogramm Eng Remote Sens 70:703–716
Schofield O, Kohut J, Glenn S (2008) Evolution of coastal observing networks. Sea Technol 49:31–36
Shearman EDR, Moorhead MD (1988) PISCES: a coastal ground-wave HF radar for current, wind, and wave mapping to 200 km ranges. In: Proceedings of IGARSS'88, Tsukuba City, Japan, pp 773–776
Simard M, Fatoyinbo LE, Pinto N (2010) Mangrove canopy 3D structure and ecosystem productivity using active remote sensing. In: Wang J (ed) Remote sensing of coastal environment. CRC Press, Boca Raton
Simis SGH (2005) Remote sensing of the cyanobacterial pigment phycocyanin in turbid inland waters. Limnol Oceanogr 50:237–245
Sinclair M (1999) Laser hydrography – commercial survey operations. In: Proceedings of US hydrographic conference, Mobile, Alabama, USA
Sinclair M (2008) Airborne LiDAR hydrographic survey for homeland security. Sea Technol 49:15–20

Skop RA, Peters NJ (1997) Shipboard deployment of a VHF OSCR system for measuring offshore currents. Oceanography 10:80–81
Smith VH (2006) Responses of estuarine and coastal marine phytoplankton to nitrogen and phosphorus enrichment. Limnol Oceanogr 51:377–384
Space Imaging (2003) IKONOS imagery products and product guide (version 1.3). Space Imaging LLC, Thornton
Stockdon HF, Sallenger AH, List JH, Holman RA (2002) Estimation of shoreline position and change using airborne topographic LiDAR data. J Coast Res 18:502–513
Stoker JM, Tyler DJ, Turnipseed DP, Van Wilson Jr K, Olmoen MJ (2009) Integrating disparate Lidar data sets for regional storm tide inundation analysis of Hurricane Katrina. J Coast Res Spec Issue 53:66–72
Stone GW, Muller RA (2005) Meteorological effects on coasts. In: Encyclopedia of coastal science. Springer, Dordrecht, pp 636–637
Stumpf RP, Tomlinson MC (2005) Remote sensing of harmful algal blooms. In: Miller R, Del Castillo C, McKee B (eds) Remote sensing of coastal aquatic environments: technologies, techniques and applications. Kluwer Academic Publishers, Dordrecht
Stumpf RP, Tomlinson MC, Calkins JA, Kirkpatrick B, Nierenberg K, Currier R, Wynne TT (2009) Skill assessment for an operational algal bloom forecast system (special issue on skill assessment of ecological oceanographic models). J Mar Syst 76:151–161
Teague CC, Vesecky JF, Fernandez DM (1997) HF radar instruments, past to present. Oceanography 10:40–44
Thompson RL, Schroeder AJJr (2010) High-definition 3-D tools for underwater surveying and inspection. Sea Technol 51:43
Trembanis AC, Hiller T, Patterson M (2008) Exploring coral reef sustainability. Hydro Int 12:10–15
Trizna DB (2007) Monitoring coastal processes and ocean wave directional spectra using a marine radar. OCEANS 2006 – Asia Pacific, pp 1–4
UCAR (2010) Ocean currents likely to carry oil along Atlantic coast. http://www2.ucar.edu/news/ocean-currents-likely-to-carry-oil-spill-along-atlantic-coast. Accessed 6 Aug/2010
Uchida H, Imawaki S (2003) Eulerian mean velocity field derived by combining drifter and satellite altimeter data. Geophys Res Lett 30:1229
Wang Y (2010) Remote sensing of coastal environments. CRC Press/Taylor and Francis Group, Boca Raton
Wang C-K, Philpot WD (2007) Using airborne bathymetric LiDAR to detect bottom type variation in shallow waters. Remote Sens Environ 106:123–135
West GR, Lillycrop WJ, Pope RW (2001) Utilization of airborne LiDAR bathymetry for rapid environmental assessment. Sea Technol 42:10–15
Wu L-C, Kao CC, Yang W-H (2010) Sea state monitoring from a mobile X-band radar system. Sea Technol 51:40–42
Yan X-H, Breaker LC (1993) Surface circulation estimation using image processing and computer vision methods applied to sequential satellite imagery. Photogramm Eng Remote Sens 59:407–413
Yang X (2009) Remote sensing and geospatial technologies for coastal ecosystem assessment and management. Springer, Berlin
Yang J, Artigas FJ (2010) Mapping salt marsh vegetation by integrating hyperspectral and LiDAR remote sensing. In: Wang J (ed) Remote sensing of coastal environment. CRC Press, Boca Raton
Yang C, Everitt JH, Fletcher RS, Jensen JR, Mausel PW (2009) Mapping black mangrove along the south Texas gulf coast using AISA + hyperspectral imagery. Photogramm Eng Remote Sens 75:425–436
Zawada DG, Brock JC (2009) A multi-scale analysis of coral reef topographic complexity using Lidar-derived bathymetry. J Coast Res Spec Issue 53:6–15